J Mater Sci: Mater Electron (2016) 27:6060–6070
DOI 10.1007/s10854-016-4531-4

Changes in mechanical and structural properties of Bi-2212 added MgB_2 superconductors

E. Taylan Koparan[1] · B. Savaskan[2] · O. Ozturk[3,4] · S. Kaya[4] · C. Aksoy[5] · J. Wang[6] · S. C. Speller[6] · C. R. M. Grovenor[6] · A. Gencer[7,8] · E. Yanmaz[9]

Received: 20 December 2015 / Accepted: 14 February 2016 / Published online: 22 February 2016
© Springer Science+Business Media New York 2016

Abstract In the present study, we investigate the effects of $Bi_2Sr_2Ca_1Cu_2O_{8+\kappa}$ (Bi-2212) addition on structural and mechanical properties of bulk MgB_2 obtained by hot-press method by means of X-ray diffraction, the Scanning Electron Microscopy and Vickers microhardness measurements. The amount of Bi-2212 was varied between 0 and 10 wt% (0, 2, 4, 6, 8 and 10 wt%) of the total MgB_2. All samples were prepared by using elemental magnesium (Mg) powder, amorphous nano boron (B) powder and Bi-2212 powder which are produced by hot-press method. As a result of the hot-press process, the compact pellet samples were manufactured. The microhardness results were analyzed by Meyer's law, Proportional Sample Resistance Model, Elastic–Plastic Deformation Model, Hays Kendall Approach, and Indentation Induced Cracking (*IIC*) Model. *IIC* model was identified as the most appropriate model for samples exhibiting the reverse indentation size effect behavior.

✉ E. Taylan Koparan
etaylan20@gmail.com

1 Department of Science Education, Ereğli Faculty of Education, Bülent Ecevit University, 67300 Ereğli, Zonguldak, Turkey

2 Energy Systems Engineering, Faculty of Technology, Karadeniz Technical University, 61830 Of, Trabzon, Turkey

3 Department of Physics, Arts and Science Faculty, Kastamonu University, 37100 Kastamonu, Turkey

4 Research and Application Center, Kastamonu University, 37100 Kastamonu, Turkey

5 Electronic and Communication Engineering, Faculty of Technology, Karadeniz Technical University, 61830 Trabzon, Turkey

6 Department of Materials, University of Oxford, Parks Road, OX1 3PH Oxford, UK

7 Department of Physics, Faculty of Science, Ankara University, 06100 Tandoğan, Ankara, Turkey

8 Center of Excellence for Superconductivity Research, Ankara University, 50 Year Campus, Golbaşı, Ankara, Turkey

9 Department of Mechatronics, Faculty of Engineering and Architecture, İstanbul Gelişim University, Istanbul, Turkey

1 Introduction

For the bulk superconductor materials, the mechanical properties are as vital as the superconducting properties like critical temperature, critical current density, and critical magnetic field for industrial applications in the form of wires and tapes [1]. Superconductivity in MgB_2, which is a binary intermetallic compound, was discovered by Akimitsu's group in 2001 [2]. The superconducting properties of MgB_2 can be improved by methods such as chemical addition or doping, thermo-mechanical processing, mechanical alloying [3], hot-press [4] or proton irradiation. Amongst these, the chemical addition and doping are simple and effective techniques to improve the superconducting properties of MgB_2 [5]. Numerous researches up to the present on chemical doping in MgB_2 have been concentrated on the addition of normal type of dopants [6]. The effects of the addition of high temperature superconductors with higher T_c than MgB_2 superconductor have rarely been studied until now [6–10]. To our best knowledge, none of these studies has been interested in the effects of Bi-2212 on the mechanical properties of MgB_2 bulk superconductors. Shen et al. [8] studied on bulk samples of MgB_2 with Bi-2212 powder addition [0, 3, 5, and 10 wt% $Bi_2Sr_2CaCu_2O_8$ (Bi-2212) particles] prepared by using conventional solid-state reaction method. They

reported that after Bi-2212 addition (which acts as repulsive pins in this system), the critical current density and flux pinning of MgB_2 bulk samples were enhanced [8]. Due to discovery of its superconductivity, use of MgB_2 compound in various technological and industrial applications has drawn attention to the mechanical properties of the material. Many scientists have carried out a lot of work to improve the mechanical properties of this material [11–17]. For these reasons, we have focused on mechanical properties of $Bi_2Sr_2Ca_1Cu_2O_{8+\kappa}$ (Bi-2212) added (from 0 to 10 wt% of the total MgB_2) into MgB_2 bulk samples via performing Vickers microhardness measurements in the current study. In addition, other mechanical parameters such as elastic modulus (E), yield strength (Y), fracture toughness (K_{IC}) were also examined.

2 Experimental details

All samples were prepared from elemental magnesium (Mg) powder (Alfa Aesar, purity 99.8 %, −325 mesh), amorphous nano boron (B) powder (supplied from Pavezyum Turkish co., purity 98.5 %) and $Bi_2Sr_2Ca_1Cu_2O_{8+\kappa}$ (Bi-2212) powder (purchased from Merck Chemical Company). Bulk MgB_2 superconductors were fabricated as described in our previous study [18]. In order to investigate the effect of Bi-2212 additions on the mechanical and structural properties of the MgB_2 bulk, Bi-2212 powder in different adding levels was added to each reacted powder (in amount of 2 g). The level of added Bi-2212 powder was 0, 2, 4, 6, 8, 10 wt% of the reacted powder (in amount of 2 g).

The phase and crystal structure of the prepared samples were investigated by Rigaku D/Max-III diffractometer with a step size of 0.02 over the range of 20°–80° using Cu K_α ($\lambda = 1.5406$ Å) target at room temperature. The MgB_2 bulk samples were mounted into the epoxy-resin then mechanically grinded and polished finely without using water. The samples were coated by carbon to make the whole sample conductive for measuring in SEM. The quantitative and microstructural analysis were made by Oxford Instruments Energy dispersive x-ray EDX detector, Jeol 5510 SEM at 20 kV and Jeol 840 F equipped Field emission gun at 5 kV. Vickers Microhardness measurements were performed to determine the mechanical properties of Bi-2212 added MgB_2 samples. Measurements were taken by Shimadzu HVM-2 model at room temperature. A pyramid-shaped indenter with different loads such as 0.245, 0.490, 0.980, 1.960 and 2.940 N were applied for loading time of 10 s and diagonals of the resultant impression were measured by an optical microscope with an accuracy of ±0.1 m. All the measurement results were compared with pure MgB_2 and Bi-2212 added MgB_2 bulk samples.

3 Results and discussion

3.1 Structural characterization

Figure 1 displays the X-ray diffraction patterns of pure and Bi-2212 superconductor added MgB_2 samples as detailed in our previous study [18]. The analysis shows that most of the reflections correspond to MgB_2 phase in all samples. Besides these reflections, different reflections were observed impurity phases as MgO, Mg. Again from these reflections, it can be seen that residual B was not detected because of its amorphous feature in all samples. The presence of MgO is expected in MgB_2 due to the strong affinity of Mg to get oxidized [5]. The peaks of unreacted Mg were formed since excess Mg was added in the precursor. The aim of using excess Mg in this preparation method was to prevent the loss of Mg during reaction and to improve rigidity of the final product of MgB_2. In addition to MgO and Mg impurity phases, some unknown peaks were detected with the increasing amounts of Bi-2212 additions. XRD patterns also indicate that Bi-2212 addition does not display any shift of the diffraction angles of MgB_2. These results suggest no Bi-2212 substitution in Mg and B sites [7, 19].

The lattice parameters of both pure and Bi-2212 superconductor added MgB_2 samples were calculated by using the following Eq. (1) for hexagonal system [20]:

$$\sin^2\theta = \frac{\lambda^2}{4}\left[\frac{4}{3}\left(\frac{h^2+hk+k^2}{a^2}\right)+\frac{l^2}{c^2}\right] \quad (1)$$

Here λ ($\lambda = 1.5406$ Å) is Cu Kα wave length, θ is peak position, h, k, l are miller index, and a, c are the lattice parameters. The lattice parameters and their ratio, unit cell

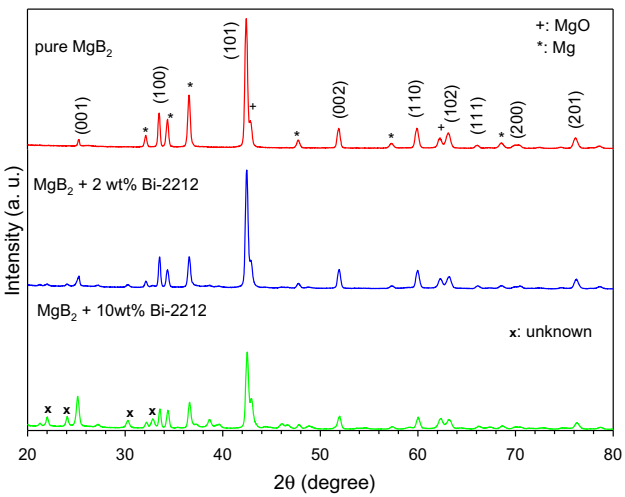

Fig. 1 The X-ray diffraction patterns for pure, 2 and 10 wt% Bi-2212 added MgB_2 samples

volume for both pure and Bi-2212 superconductor added MgB_2 samples are listed in Table 1. It is seen in the Table 1 that there is no significant change in lattice parameters and c/a ratio for Bi-2212 added MgB_2 samples and hence this shows absence of substitution effect [6].

As shown in Fig. 2, SEM images showed that the particle size of the MgB_2 sample was mostly distributed around between 900 nm and 6 μm (micro scale) and showed randomly oriented hexagonal MgB_2 grains with clear grain boundaries. All samples seemed to have high porosity between the contributed atoms.

Table 1 Lattice parameters and their ratio, unit cell volume for pure and Bi-2212 superconductor added MgB_2 samples

Samples	Lattice parameters			Volume (Å^3)
	a = b (Å)	c (Å)	c/a	
Pure MgB_2	3.0886	3.5239	1.1409	29.1124
2 wt% Bi-2212	3.0858	3.5213	1.1411	29.0382
4 wt% Bi-2212	3.1005	3.5449	1.1433	29.5120
6 wt% Bi-2212	3.0769	3.5110	1.1411	28.7865
10 wt% Bi-2212	3.0822	3.5287	1.1449	29.0313

The EDX layered image and maps of the pure MgB_2 sample indicated that Mg, B, O atoms distributed randomly. Mg has the highest volume fraction as high content of Mg added to the sample during the sample preparation process to prevent the loss of Mg during reaction and to improve rigidity of the final product of MgB_2. Unreacted Mg peaks were also detected at the XRD data. Therefore, it can be seen from the Fig. 3 maps that MgO also was segregated as the two-step heat treatment method was applied during the sample preparation process.

As seen in Fig. 4, the EDX layered image and elemental maps of the 2 wt% Bi-2212 added MgB_2 sample revealed that Bi, Ca and Sr were separated from Bi-2212 structure. It might be because of the higher sintering temperature of the process as the general process temperature of Bi-2212 is 850 °C. However, in this study a different sintering method was applied at 1000 °C. We thought that the higher sintering temperature may destroy the Bi-2212 structure. The melted Bi-2212 atoms at 1000 °C might diffuse into the pores and might affect the MgB_2 structure. The Fig. 5 showed clearly that Sr and Bi segregated completely and there is no sign for Bi-2212 structure in the 10 wt% Bi-2212 added MgB_2 sample.

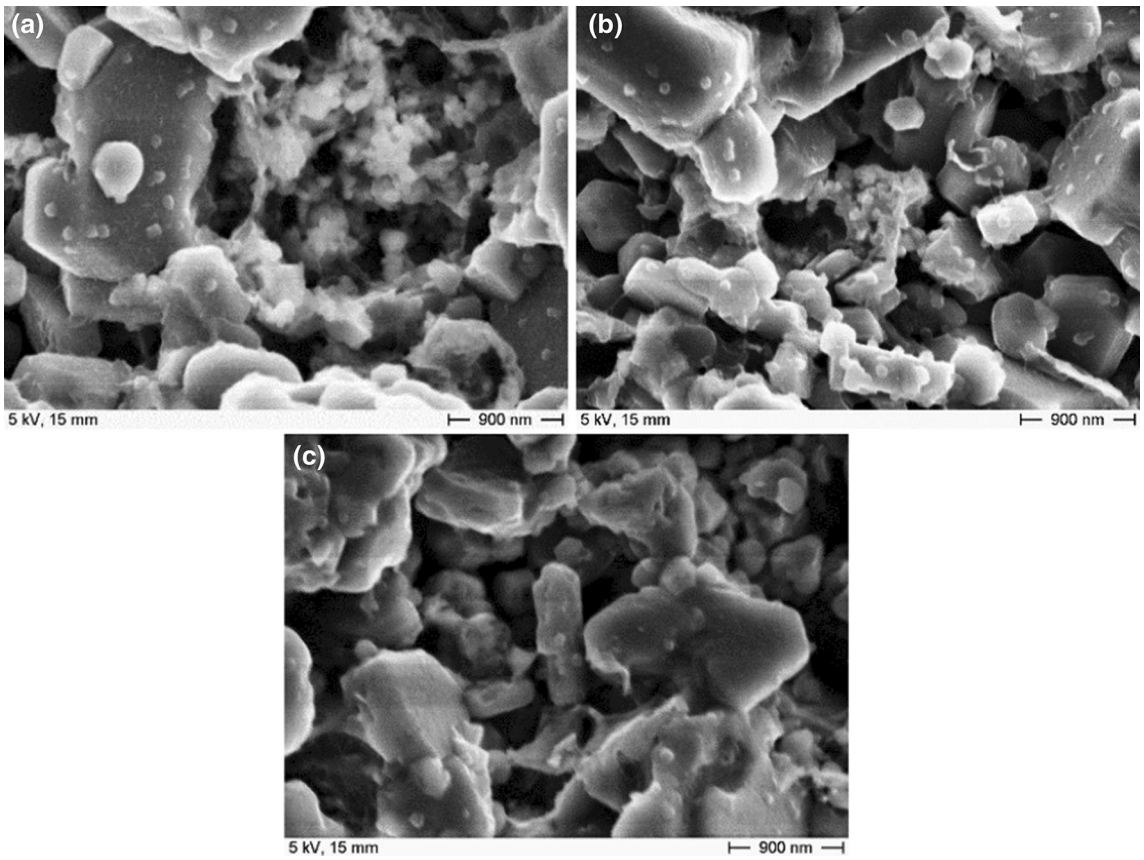

Fig. 2 SEM images of **a** pure MgB_2, **b** 2 wt% Bi-2212 added and **c** 10 wt% Bi-2212 added MgB_2 samples

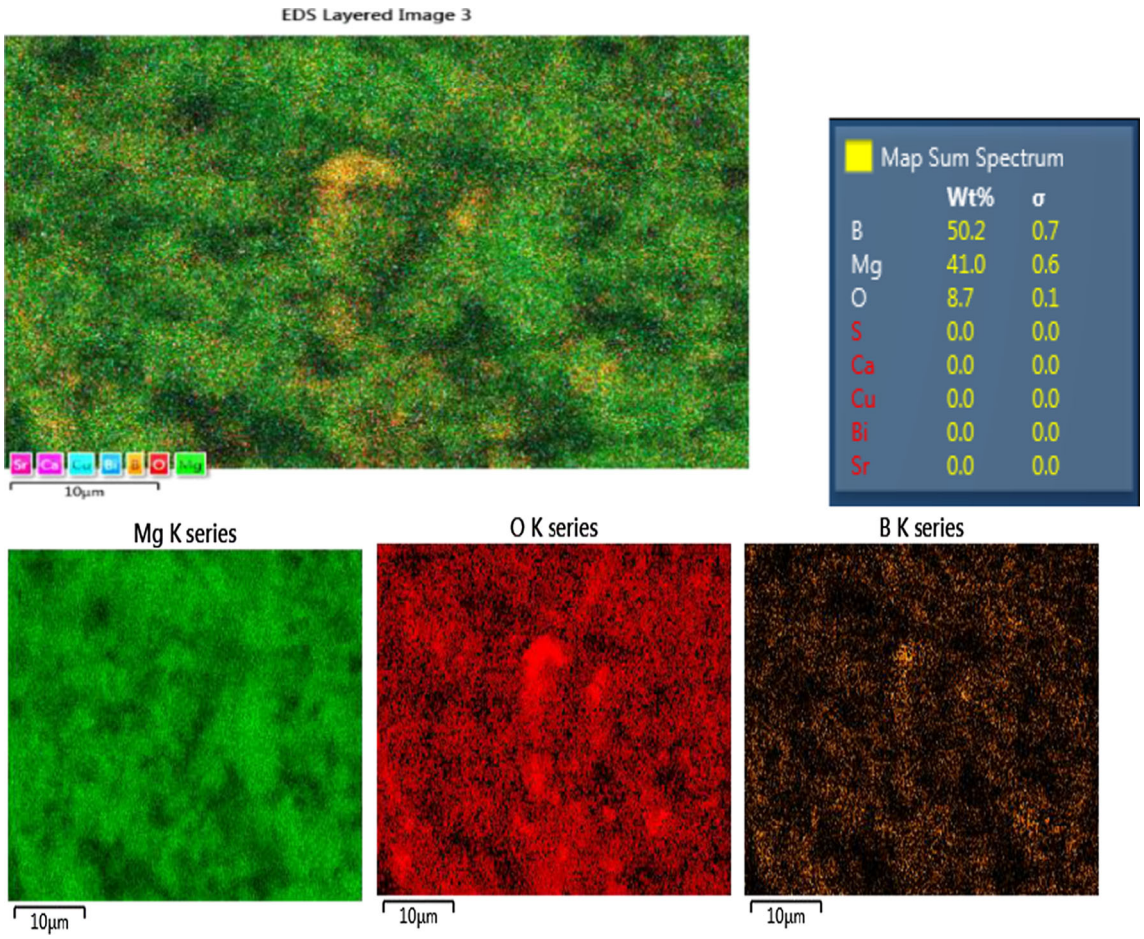

Fig. 3 EDX layered image and elemental maps of the pure MgB_2 sample

3.2 Mechanical characterization

In order to investigate mechanical properties of the samples, Vickers microhardness was used in this study. As it is known, Vickers microhardness test is performed by applying a controlled load for standard period of time with a square-based diamond pyramid indenter and then the indenter is removed. The diagonal of the resultant impression is measured with a microscope. The Vickers microhardness values of the samples are calculated by using a specific formula as presented in Eq. (2),

$$H_V = 1854.4\left(F/d^2\right) \quad \text{(GPa)} \tag{2}$$

Here, H_v denotes the Vickers microhardness, F is the applied load in N, d is the diagonal length of indentation in µm. The Vickers microhardness (H_V) values, elastic modulus (E), yield strength (Y), fracture toughness (K_{IC}) values are calculated by using Eqs. (3–5) for all samples given in Table 2.

$$E = 81.9635\, H_V \tag{3}$$

$$Y \approx H_V/3 \tag{4}$$

$$K_{IC} = \sqrt{2E\gamma}$$
(γ : surface energy is calculated using PSR model(a_1)) (5)

The variation in load-dependent microhardness as a function of the applied load for all the samples is shown in Fig. 6. From the figure, it can be said that microhardness values strongly depend on indentation applied load and dopant. Also, the microhardness values of the samples are given in Table 2. From the table, it can be said that microhardness values increase with the increasing indentation load. This behavior is defined as reverse indentation size effect (*RISE*) in the literature [21–23]. In addition to this, other mechanical parameters such as elastic modulus (E), fracture toughness (K_{IC}), yield strength (Y) are calculated by Vickers microhardness measurements (Table 2). It is seen that all these mechanical parameters increased with the increasing applied load and Bi-2212 adding.

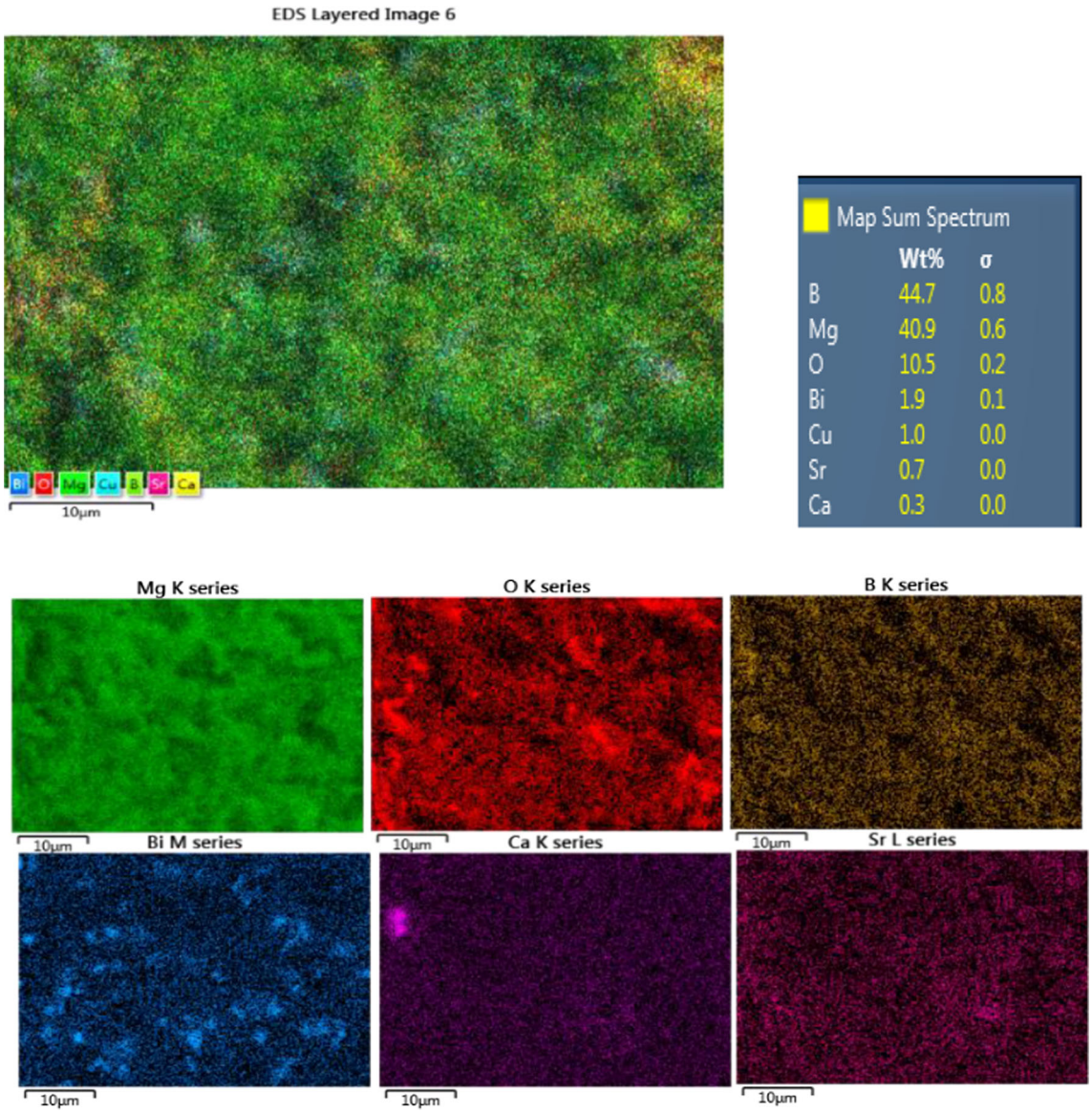

Fig. 4 EDX layered image and elemental maps of the 2 wt% Bi-2212 added MgB_2 sample

There are different models to describe the load dependence of the samples such as Meyer Law, Proportional Sample Resistance (*PSR*) Model, Elastic/Plastic Deformation Model (*EPD*) Hays-Kendall (*HK*) Model, and Indentation Induced Cracks (*IIC*) model [24–29]. In order to analyse microhardness results, all these models have been applied to the samples whose results are listed below.

3.2.1 Meyer law

Meyer's Law is an empirical equation which is used to describe ISE and RISE behavior. It exhibits the correlation between indentation applied load and resultant indentation size using the following equation [30],

$$F = Ad^n \tag{6}$$

where A and n (Meyer index) are the constants obtained from curve fitting of experimental data. The ''n'' value plays an important role in describing ISE and RISE behaviors in the samples. In addition, the values of ''n'' obtained from the Fig. 7 are shown in Table 3. According to the table, the ''n'' values of all the samples are higher than 2 confirming RISE behavior of the samples.

3.2.2 PSR model

Proportional Specimen Resistance (PSR) model suggests a relationship between the applied indentation load and the

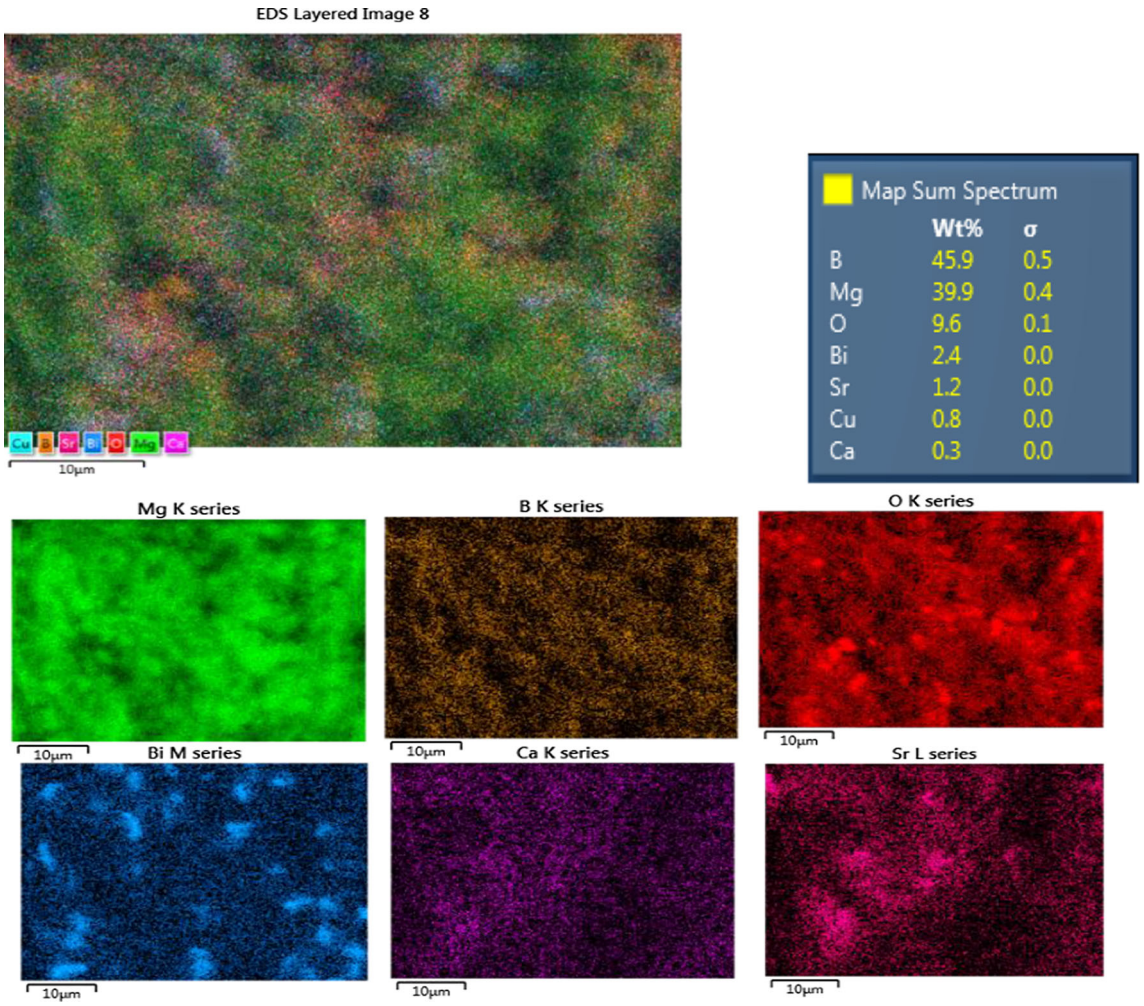

Fig. 5 EDX layered image and elemental maps of the 10 wt% Bi-2212 added MgB_2 sample

resultant indentation size [31]. This relationship can be written as

$$F = a_1 d + a_2 d^2 \tag{7}$$

where a_1 and a_2 are constants related to the sample. In PSR model, the hardness value is calculated by the following equation

$$H_{PSR} = 1884.4\, a_2 \tag{8}$$

Figure 8 shows the variation of F/d versus d of the samples. The calculated hardness values of PSR model are given in Table 4. The load-independent elastic modulus (E_o), stress (Y_o), fracture toughness (K_{IC}) values are also given in Table 5. As seen from the tables, the hardness values of the sample increased with the increasing adding concentration. In addition, calculated load-independent PSR hardness values as well as (E_o), (Y_o) and (K_{IC}) are quite far from the load dependent hardness value. So that, PSR model is not sufficient to explain the microhardness values of the samples.

3.2.3 EPD model

In Elastic/Plastic Deformation EPD Model, the dependence of indentation size on the applied load is defined by the following equation [32]

$$F^{1/2} = A_1^{1/2} d_p + A_2^{1/2} d_e \tag{9}$$

where A_1 and A_2 are constant, d_e is a correction term added to d_p since elastic recovery occurs around the indentation trace after removing the indenter. Figure 9 shows the applied indentation load dependence of the indentation diagonals of the samples. In EPD model, the hardness value is calculated by the following equation

$$H_{EPD} = 1854.4\, A_2 \tag{10}$$

Table 2 The load dependent H_v, E, Y and K_{IC} for the samples

Samples	Load (N)	H_v (GPa)	E (GPa)	Y (GPa)	K_{ic} (Pa/m$^{1/2}$)
Pure MgB_2	0.245	0.165	13.523	0.055	34.46
	0.490	0.242	19.835	0.080	41.74
	0.980	0.389	31.883	0.129	52.92
	1.960	0.472	38.686	0.157	58.28
	2.940	0.485	39.752	0.161	59.09
2 wt% Bi-2212	0.245	0.194	15.900	0.064	45.46
	0.490	0.284	23.277	0.094	54.99
	0.980	0.487	39.916	0.162	72.02
	1.960	0.610	49.997	0.203	80.60
	2.940	0.654	53.604	0.218	83.47
4 wt% Bi-2212	0.245	0.255	20.900	0.085	49.41
	0.490	0.312	25.572	0.104	54.65
	0.980	0.521	42.702	0.173	70.63
	1.960	0.652	53.440	0.217	79.01
	2.940	0.662	54.259	0.220	79.61
6 wt% Bi-2212	0.245	0.306	25.080	0.102	55.20
	0.490	0.356	29.179	0.118	59.53
	0.980	0.570	46.719	0.190	75.34
	1.960	0.712	58.358	0.237	84.20
	2.940	0.721	59.095	0.240	84.73
8 wt% Bi-2212	0.245	0.413	33.850	0.137	63.85
	0.490	0.491	40.244	0.163	69.61
	0.980	0.652	53.440	0.217	80.22
	1.960	0.797	65.324	0.265	88.69
	2.940	0.802	65.734	0.267	88.97
10 wt% Bi-2212	0.245	0.491	40.244	0.163	73.29
	0.490	0.594	48.686	0.198	80.61
	0.980	0.720	59.013	0.240	88.75
	1.960	0.901	73.849	0.300	99.28
	2.940	0.915	74.996	0.305	100.05

All the calculated load-independent microhardness values and d_e are listed in Table 6. It is clear from the table that all the microhardness values increased with the increasing adding concentration. Besides, it can be said that all the d_e values are negative confirming no elastic deformation. Considering the H_{EPD} values given in Table 6, it can be said that EPD Model is not suitable for describing microhardness values of the samples.

3.2.4 HK approach

Hays and Kendall have pointed out that there exists a minimum load value (W_{HK}) to create a permanent deformation in the material. If the applied load does not exceed this resistance, permanent deformation does not occur and only elastic deformation takes place [33]. And they suggested that experimentally obtained indentation diagonal length is proportional to an effective load ($F_{eff.}$) instead of the applied load (F)

$$F - W_{HK} = A_{1HK} d^2 \tag{11}$$

where W_{HK} is the minimum applied load to create indentation, and A_{1HK} is the load-independent hardness constant. In this model, hardness value is calculated by the following equation

$$H_{HK} = 1854.4\, A_{1HK} \tag{12}$$

$F - d^2$ graph and W_{HK}, A_{1HK} and H_{HK} values calculated are given in Fig. 10 and Table 7, respectively. From the Table 7, it is seen that the W_{HK} value is negative for all the samples confirming RISE behavior in the samples. This means that the applied load is enough to create both elastic and plastic deformations [34]. In addition, it is seen from the table that the H_{HK} values of the samples are not close to the H_v values of the samples (Table 7). So, it does not

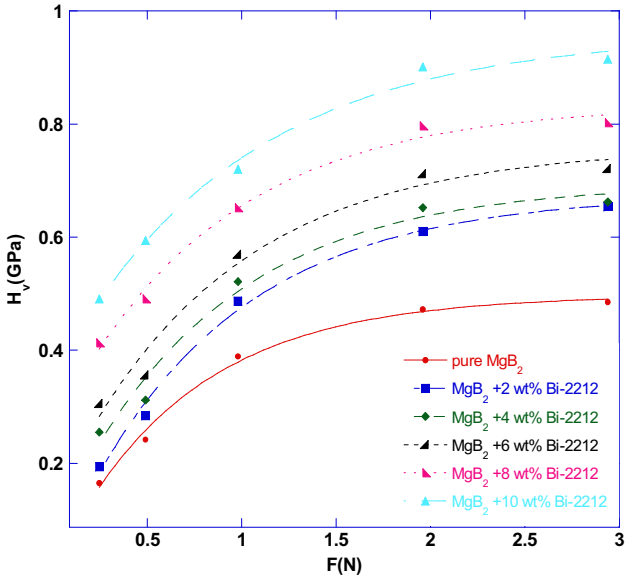

Fig. 6 The variations of microhardness values (H_V) with applied load

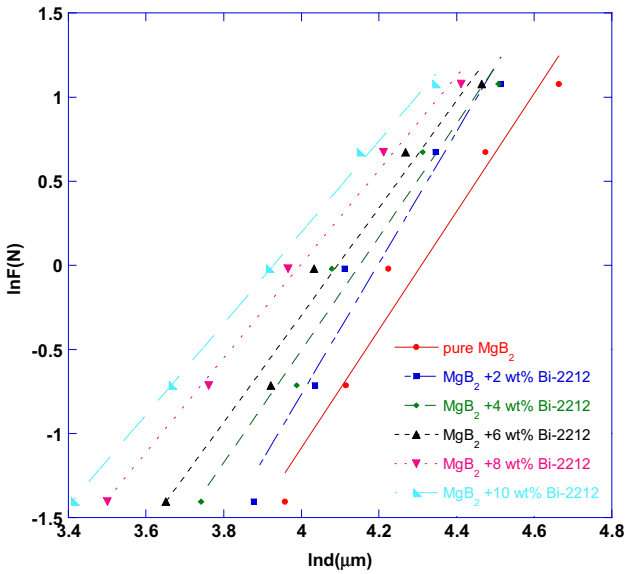

Fig. 7 Variation of *lnF* with *lnd* for the samples

make sense to explain the hardness value of the samples by Hays-Kendall model.

3.2.5 IIC model

The Indentation-Induced Cracking model is reported by Li and Bradt [35] in order to study RISE behavior in the sample. According to Li and Bradt, applied load is balanced by the total resistance which consists of friction at the indenter/specimen facet interface (R_e), elastic deformation (R_f), plastic deformation (R_p), and specimen cracking (R_c). This total resistance can be expressed as

$$F = R_e + R_f + R_p + R_c \tag{13}$$

where F is the applied test load. In this model hardness can be defined by the following expression

$$H_v = \lambda_1 K_1 \left(\frac{F}{d^2}\right) + K_2 \left(\frac{F^{5/3}}{d^3}\right) \tag{14}$$

where d is the diameter of the trace, and λ_1, K_1, and K_2 are constants. While K_2 is load-dependent, K_1 is a constant dependent on the indenter geometry. For ideal plastic materials, $\lambda_1 = 1$, $K_2 = 0$; but for perfect brittle solids $\lambda_1 = 0$. If the sample being tested is fragile, only the second portion of the equation is used. In this study, the second part of the equation is used due to elastic deformation of all samples. Starting from here, the hardness value of all samples can be calculated by the equation below

Table 3 Regression analysis of the experimental data according to Meyer's law

Samples	Slope n_k	$\ln_{Ak}$ (GPa)
Pure MgB_2	3.513	−15.139
2 wt% Bi-2212	3.908	−16.402
4 wt% Bi-2212	3.368	−13.978
6 wt% Bi-2212	3.182	−13.024
8 wt% Bi-2212	2.798	−11.987
10 wt% Bi-2212	2.713	−10.658

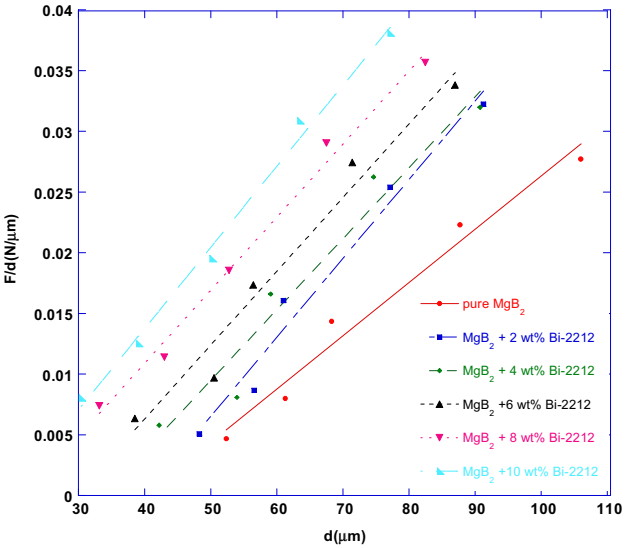

Fig. 8 Plots of *F/d* versus *d* for the samples

Table 4 Regression analysis of the experimental data according PSR Model

Samples	$a_1 \times 10^{-3}$ (N)	$a_2 \times 10^{-5}$ (N/μm)	H_{PSR} (GPa)	H_V (GPa)
Pure MgB_2	−17.59	43.92	0.814	0.472–0.485
2 wt% Bi-2212	−25.97	64.99	1.224	0.610–0.654
4 wt% Bi-2212	−19.71	58.42	1.100	0.652–0.662
6 wt% Bi-2212	−18.01	60.76	1.144	0.712–0.721
8 wt% Bi-2212	−13.17	60.22	1.134	0.797–0.802
10 wt% Bi-2212	−12.94	66.75	1.257	0.901–0.915

Table 5 The load independent H_o, E_o, Y_o, K_{IC} values for the samples

Samples	H_0 (GPa)	E_0 (GPa)	Y_0 (GPa)	K_{ic} (Pa/$m^{1/2}$)	H_v (GPa)
Pure MgB_2	0.814	66.71	0.271	76.483	0.472–0.485
2 wt% Bi-2212	1.224	100.32	0.408	114.191	0.610–0.654
4 wt% Bi-2212	1.100	90.15	0.366	102.631	0.652–0.662
6 wt% Bi-2212	1.144	93.76	0.381	106.74	0.712–0.721
8 wt% Bi-2212	1.134	92.94	0.378	105.80	0.797–0.802
10 wt% Bi-2212	1.257	103.02	0.419	117.27	0.901–0.915

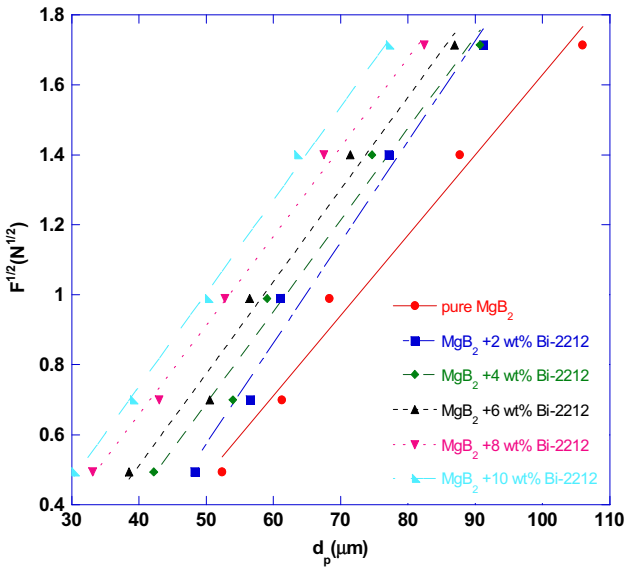

Fig. 9 Plots of $F^{1/2}$ versus d_p for the samples

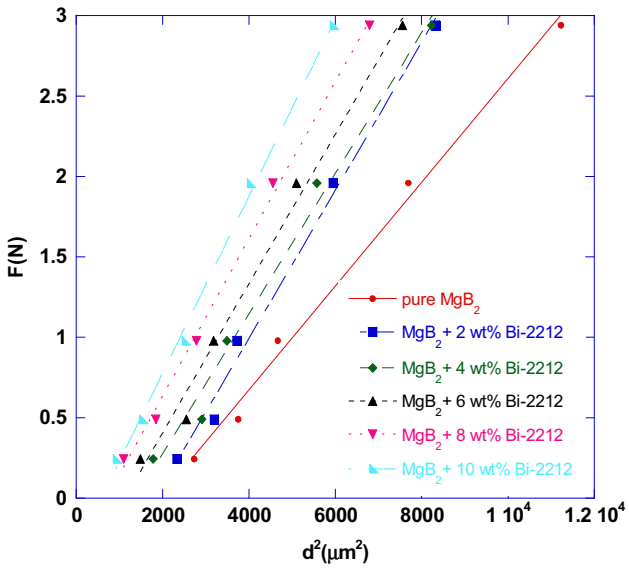

Fig. 10 Plots of F versus d^2 for the samples

Table 6 Regression analysis of the experimental data according EPD Model

Samples	$A_2^{1/2}$	d_e (μm)	H_{EPD} (GPa)	H_v (GPa)
Pure MgB_2	0.022	−0.663	0.897	0.472–0.485
2 wt% Bi-2212	0.028	−0.862	1.453	0.610–0.654
4 wt% Bi-2212	0.026	−0.619	1.253	0.652–0.662
6 wt% Bi-2212	0.026	−0.541	1.253	0.712–0.721
8 wt% Bi-2212	0.025	−0.361	1.159	0.797–0.802
10 wt% Bi-2212	0.026	−0.329	1.253	0.901–0.915

$$H_v = K\left(\frac{F^{5/3}}{d^3}\right)^m \tag{15}$$

where K and m values are independent of load obtained using $ln(H_v)$ versus $ln(F^{5/3}/d^3)$ graph. Also, index m is an indication of either the ISE or RISE behavior in the material ($m > 0.6$ normal ISE, $m < 0.6$ RISE) [21, 35]. $ln(H_v)$ versus $ln(F^{5/3}/d^3)$ graph and hardness values calculated are given in Fig. 11 and Table 8, respectively. In addition to these, all the comparative hardness values calculated based on applied models are given in Table 9. It is clear from the table that *IIC* model hardness values are close to hardness values of the plateau region for all

Table 7 Regression analysis of the experimental data according to *HK* model

Samples	$A_{1HK} \times 10^{-5}$	W_{HK} (N)	H_{HK} (GPa)	H_v (GPa)
Pure MgB_2	32.24×10^{-5}	−0.617	0.597	0.472–0.485
2 wt% Bi-2212	45.90×10^{-5}	−0.837	0.851	0.610–0.654
4 wt% Bi-2212	43.57×10^{-5}	−0.593	0.807	0.652–0.662
6 wt% Bi-2212	46.38×10^{-5}	−0.521	0.860	0.712–0.721
8 wt% Bi-2212	48.75×10^{-5}	−0.342	0.904	0.797–0.802
10 wt% Bi-2212	54.96×10^{-5}	−0.321	1.091	0.901–0.915

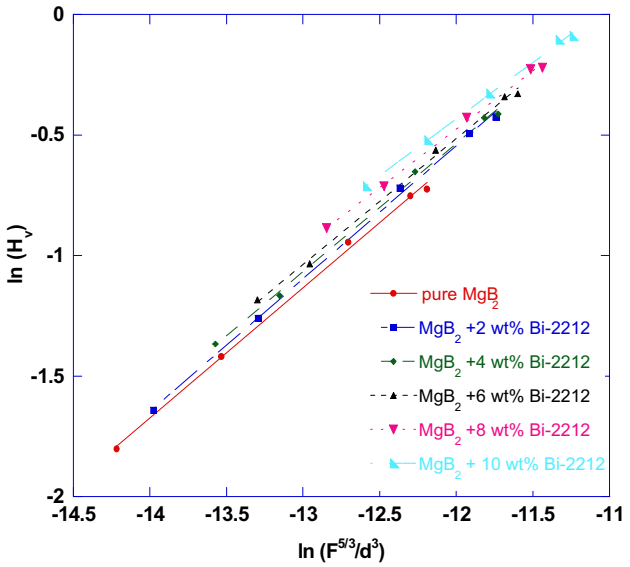

Fig. 11 Plots of $ln(H_V)$ versus $ln(F^{5/3}/d)^3$ according to *IIC* model for the samples

samples. As a result, *IIC* Model is the most appropriate model for the Bi-2212 added MgB_2 samples.

4 Conclusion

With this study, as different from the literature the effects of Bi-2212 addition on the mechanical properties of bulk MgB_2 superconductors were reported. XRD patterns indicate that there is no significant change in lattice parameters and c/a ratio for Bi-2212 added MgB_2 samples and hence this shows absence of substitution effect. SEM images showed that hexagonal MgB_2 grains with clear grain boundaries oriented randomly. All samples seemed to have high porosity between the contributed atoms. Increasing adding amount caused an increase in porosity. Namely, pores and cracks increased. Microhardness measurements clearly show that (Fig. 6) melted Bi-2212 structure fills these cracks and pores which cause regular increase in the hardness of the samples. The EDX layered image and

Table 8 Regression analysis of the experimental data according to IIC model

Samples	m	$K \times 10^4$ [$N^{(3-5m)/3}/\mu m^{(2-3m)}$]	H_{IIC} (GPa)	H_v (GPa)
Pure MgB_2	0.54	5.89	0.349	0.472–0.485
2 wt% Bi-2212	0.55	6.06	0.438	0.610–0.654
4 wt% Bi-2212	0.53	5.85	0.481	0.652–0.662
6 wt% Bi-2212	0.52	5.74	0.538	0.712–0.721
8 wt% Bi-2212	0.48	5.34	0.638	0.797–0.802
10 wt% Bi-2212	0.47	5.21	0.713	0.901–0.915

Table 9 The results of load dependent Vickers microhardness at the plateau region and load independent hardness values calculated using *PSR*, *EPD*, *HK* and *IIC* models

Samples	H_{PSR} (GPa)	H_{EPD} (GPa)	H_{HK} (GPa)	H_{IIC} (GPa)	H_v (GPa)
Pure MgB_2	0.814	0.897	0.597	0.349	0.472–0.485
2 wt% Bi-2212	1.224	1.453	0.851	0.438	0.610–0.654
4 wt% Bi-2212	1.100	1.253	0.807	0.481	0.652–0.662
6 wt% Bi-2212	1.144	1.253	0.860	0.538	0.712–0.721
8 wt% Bi-2212	1.134	1.159	0.904	0.638	0.797–0.802
10 wt% Bi-2212	1.257	1.253	1.091	0.713	0.901–0.915

elemental maps revealed that Bi, Ca and Sr were separated from Bi-2212 structure and segregated. It might be because of higher sintering temperature of the process as the general process temperature of Bi-2212 is 850 °C. However, in this study a different sintering method was applied at 1000 °C. According to Vickers Microhardness measurements, it is seen that all the hardness values are load dependent. All the samples show the RISE behavior which is described as increasing hardness values with increasing applied load. The melted Bi-2212 phase might diffuse into the pores or cracks and might affect the increase of the hardness in the surface of MgB_2 structure. Moreover, all the results of the Vickers Microhardness measurements are analysed by different models such as; Meyer Law, proportional sample resistance (*PSR*) model, Elastic/Plastic Deformation Model, Hays-Kendall (*HK*) Model and Indentation Induced Cracks (*IIC*) model. *IIC* model is found to be the most suitable model to analyze Bi-2212 added MgB_2 produced in this study.

Acknowledgments This work was supported by the Scientific Research Coordination Unit of Bulent Ecevit University of Turkey, with Project No. 2013-76962555-03. Vickers Microhardness measurements were carried out at research laboratory in Kastamonu University, Department of Physics.

References

1. O. Ozturk, M. Erdem, E. Asikuzun, O. Yildiz, G. Yildirim, A. Varilci, C. Terzioglu, J. Mater. Sci. Mater. Electron. **24**, 230–238 (2013)
2. J. Nagamatsu, N. Nakagawa, T. Muranaka, Y. Zentiani, J. Akimitsu, Nature **410**, 63–64 (2001)
3. E. Yanmaz, B. Savaskan, M. Basoglu, E.T. Koparan, N.R. Dilley, C.R.M. Grovenor, J. Alloys Compd. **480**, 203–207 (2009)
4. K. Shinohara, T. Futatsumori, H. Ikeda, Phys. C **468**, 1369–1371 (2008)
5. D. Tripathi, T.K. Dey, Phys. C **507**, 1–9 (2014)
6. D. Tripathi, T.K. Dey, J. Alloys Compd. **607**, 264–273 (2014)
7. D. Tripathi, T.K. Dey, J. Alloys Compd. **618**, 56–63 (2015)
8. T.M. Shen, G. Li, X.T. Zhu, C.H. Cheng, Y. Zhao, Supercond. Sci. Technol. **18**, L49–L52 (2005)
9. X.F. Rui, X.F. Sun, X.L. Xu, L. Zhang, H. Zhang, Int. J. Mod. Phys. B **19**, 375–377 (2005)
10. Y.Y. Xu, J. Ren, S.H. Han, H. Zhang, Int. J. Mod. Phys. B **21**, 3352–3354 (2007)
11. U. Kölemen, J. Alloys Compd. **425**, 429–435 (2006)
12. A. Gümbel, J. Eckert, G. Fuchs, K. Nenkov, K.-H. Müller, L. Schultz, Appl. Phys. Lett. **80**, 2725–2727 (2002)
13. N. Güçlü, Mater. Chem. Phys. **101**, 470–474 (2007)
14. H. Kitaguchi, H. Kumakura, K. Togano, Phys. C **363**, 198–201 (2001)
15. O. Gorur, M. Nursoy, C. Terzioglu, A. Varilci, I. Belenli, J. Phys. Conf. Ser. **153**, 012012 (2009)
16. O. Ozturk, E. Asikuzun, S. Kaya, M. Erdem, S. Safran, A. Kilic, C. Terzioglu, J. Supercond. Nov. Magn. **28**, 1943–1952 (2015)
17. O. Ozturk, E. Asikuzun, S. Kaya, J. Mater. Sci. Mater. Electron. **26**(6), 3840–3852 (2015)
18. E. Taylan Koparan, B. Savaskan, S.B. Guner, S. Celik, Appl. Phys. A (2016). doi:10.1007/s00339-016-9610-0
19. Y. Takikawa, M. Takeda, M. Migita, M. Uehara, T. Kuramoto, Y. Kimishima, Phys. C **471**, 905–907 (2011)
20. C. Suryanarayana, M.G. Norton, *X-Ray Diffraction: A Practical Approach* (Springer, New York, 1998), p. 126
21. K. Sangwal, Mater. Chem. Phys. **63**, 145–152 (2000)
22. J. Gong, H. Miao, Z. Zhao, Z. Guan, Mater. Sci. Eng. A **303**, 179 (2001)
23. B. Basu, N. Mukhopadhyay, K. Manisha, J. Eur. Ceram. Soc. **29**, 801 (2009)
24. L. Arda, O. Ozturk, E. Asikuzun, S. Ataoglu, Powder Technol. **235**, 479–484 (2013)
25. M. Tosun, S. Ataoglu, L. Arda, O. Ozturk, E. Asikuzun, D. Akcan, O. Cakiroglu, Mater. Sci. Eng. A **590**, 416–422 (2014)
26. E. Asikuzun, O. Ozturk, H.A. Cetinkara, G. Yildirim, A. Varilci, M. Yılmazlar, C. Terzioglu, J. Mater. Sci. Mater. Electron. **23**, 1001–1010 (2012)
27. B. Ozkurt, J. Supercond. Nov. Magn. **27**, 2407–2414 (2014)
28. H. Koralay, A. Arslan, S. Cavdar, O. Ozturk, E. Asikuzun, A. Gunen, A.T. Tasci, J. Mater. Sci. Mater. Electron. **24**, 4270–4278 (2013)
29. H. Aydın, A. Babanli, S.P. Altintas, E. Asikuzun, N. Soylu, O. Ozturk, M. Dogruer, C. Terzioglu, G. Yildirim, J. Mater. Sci. Mater. Electron. **24**, 4566–4573 (2013)
30. G. Constantinidis, R.D. Tomlinson, H. Neumann, Mag. Lett. **57**, 91 (1988)
31. H. Li, R.C. Bradt, J. Mater. Sci. **28**, 917 (1993)
32. M.L. Tarkanian, J.P. Neumann, L. Raymond, in *The Science of Hardness Testing and its Research Applications*, ed. by J.H. Westbrook, H. Conrad (American Society for Metals, Metal Park, OH, 1973), pp. 187–198
33. C. Hays, E.G. Kendall, Metallography **6**, 275–282 (1973)
34. R. Awad, A.I. Abou-Aly, M. Kamal, M. Anas, J. Supercond. Nov. Magn. **24**, 1947–1956 (2011)
35. H. Li, R.C. Bradt, J. Mater. Sci. **31**, 1065–1070 (1996)